ACS NANO

www.acsnano.org

ARTICLE

Force Volume Atomic Force Microscopy–Infrared for Simultaneous Nanoscale Chemical and Mechanical Spectromicroscopy

Martin Wagner,* Qichi Hu, Shuiqing Hu, Cassandra Phillips, Weijie Wang, Bede Pittenger, Alireza Fali, Chunzeng Li, Jérémie Mathurin, Alexandre Dazzi, Chanmin Su, and Peter De Wolf

Cite This: *ACS Nano* 2025, 19, 18791–18803

Read Online

ACCESS | Metrics & More | Article Recommendations | Supporting Information

ABSTRACT: **Photothermal atomic force microscopy–infrared (AFM-IR) combines the nanoscale spatial resolution of AFM with the chemical identification capability of infrared spectroscopy and has thrived in various applications. Currently executed in three major AFM modes (contact, tapping, and peak force tapping) we introduce a fourth variant built upon force volume mode comprising a defined engage, hold, and retract segment in each pixel. IR laser pulsing at a probe resonance frequency during the constant-force hold segment duplicates the resonance-enhanced AFM-IR detection principle of contact mode. However, force volume AFM-IR removes the lateral forces that cause tip wear and sample damage while adding the spatial resolution of tapping AFM-IR. As demonstrated on different materials, this imaging and spectroscopy technique integrates monolayer sensitivity, sub-10 nm spatial chemical resolution, simultaneous nanomechanical property sensing, and precise force control. The ability to sweep the infrared laser repetition rate in each pixel provides additional, rich information in the form of contact resonance curves, while compensating for mechanically induced probe resonance shifts in an alternative to conventional phase-locked loop based frequency tracking. Such sweeps inherently consider the Q-factor (*i.e.*, mechanical damping) in the AFM-IR response, a little investigated aspect. Furthermore, the probing depth can be varied by selecting different resonances recorded within a single broad frequency sweep. Switching to the surface sensitive AFM-IR detection scheme during the hold segment additionally limits the probing depth. These qualities should position force volume AFM-IR as a valuable addition to established AFM-IR modes.**

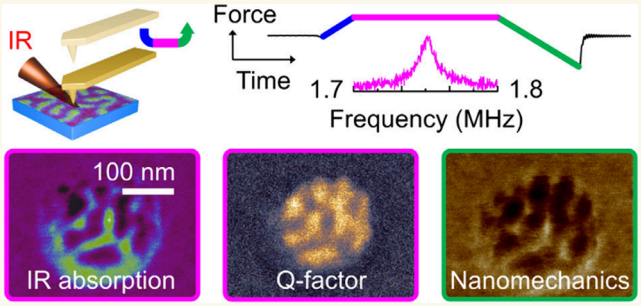

KEYWORDS: *AFM-IR, photothermal, infrared nanospectroscopy, force volume, nanomechanical, contact resonance, Q-factor*

Access to nanoscale infrared spectroscopy for material identification at length scales below the Abbe diffraction limit is crucial in many areas of science and technology. Photothermal atomic force microscopy–infrared (AFM-IR) is one of the few existing techniques in this regard besides tip enhanced Raman spectroscopy (TERS) and scattering scanning near-field optical microscopy (sSNOM). In AFM-IR an AFM probe with a tip radius of typically 10–30 nm is positioned on the sample of interest. When illuminated with infrared light, changes in the probe deflection caused by infrared sample absorption are detected with sub-10 nm spatial resolution.[1−3] Compared to TERS or sSNOM, the photothermal AFM-IR technique is especially suited for routine measurements thanks to its model-free, relatively simple and hence robust and reliable operation. It found numerous applications in diverse fields such as biology,[4−6] chemistry,[7,8] physics,[9,10] material sciences,[11,12] geology,[13] or the study of extraterrestrial matter.[14] To date photothermal AFM-IR has been incorporated into three major AFM operational modes as described in more detail below: resonance enhanced (RE) AFM-IR is based on contact mode, tapping AFM-IR on tapping mode, and peak force IR (PFIR) utilizes peak force tapping.

Received: March 6, 2025
Revised: April 29, 2025
Accepted: April 30, 2025
Published: May 12, 2025

The original photothermal AFM-IR technique was implemented in contact mode where the infrared light source (a laser) was pulsed at a repetition rate off-resonant with the AFM probe. A major improvement in sensitivity was realized by employing signal enhancement by the probe's Q-factor for resonant driving of a contact resonance mode, *i.e.* the laser repetition rate matches a cantilever mode.[15] In a more recent variation, the laser driven cantilever oscillation is suppressed *via* a subsample piezo oscillation in order to reduce mechanical noise.[16] However, built upon contact mode, such resonance enhanced AFM-IR exhibits lateral forces. This imposes limitations on soft and fragile samples despite some impressive achievements for such specimen.[5,17]

Tapping AFM-IR[18,19] based on tapping mode AFM operation is much more suited for delicate samples since lateral forces are avoided. Whereas in resonance enhanced AFM-IR the light source is pulsed at a resonance of the probe, in tapping AFM-IR the laser does not directly drive any cantilever resonance. To monitor the nonlinear interaction between the tip and the surface a heterodyne detection is used: the probe is usually tapping at the second cantilever mode while the infrared signal is read out at the first mode. The infrared laser repetition rate is then tuned to the difference frequency between the two involved resonances. This heterodyne detection process has proved very sensitive[8] and routinely achieves sub-10 nm spatial resolution on soft and fragile samples.[19−21] Some works propose the root cause for the detected cantilever deflection change in the tapping AFM-IR configuration as photoinduced dipole−dipole forces at infrared wavelengths.[20] However, several studies[22−25] contradict that assignment. They point to photothermal expansion as dominating signal origin in the infrared spectral region for most dielectric materials such as polymers or biological matter (weak oscillators with real part of the dielectric function $\varepsilon_1 > 0$). The exact source of the signal on strong oscillators ($\varepsilon_1 < 0$), *e.g.* plasmonic resonances, is still being explored.[26,27]

Recently, surface sensitive AFM-IR combined some features of aforementioned AFM-IR techniques. Built upon contact mode it utilizes heterodyne excitation as in tapping AFM-IR: a piezo actuator mechanically drives a typically higher order probe resonance while IR detection occurs at a lower order contact resonance with laser pulsing set to the difference frequency. This nonlinear acoustic wave mixing at high laser repetition rates ensures a probing depth much lower than resonance enhanced AFM-IR and below that of tapping AFM-IR.[2,28−30]

The last major AFM-IR variant, Peak force IR (PFIR),[31] utilizes peak force tapping (PFT)[32−34] as its AFM base mode. A probe is oscillated sinusoidally in and out of contact with a sample at typically 2−4 kHz, and the light induced sample response is extracted during the tip−sample contact time. Either a single laser pulse per PFT cycle can be used (as in the original PFIR experiments[35]) or continuous laser pulsing at the probe's resonance for resonance enhancement.[36] In contrast to aforementioned modalities, PFIR allows precise force control between tip and sample and additionally provides access to quantitative nanomechanical information inherent to peak force tapping.

Most AFM-IR techniques employ resonance enhancement. It necessitates matching the laser repetition rate with a probe resonance frequency for homodyne detection or maintaining a fixed frequency mixing relationship for heterodyne detection. That poses a challenge since the probe resonance is a function of the local sample stiffness, resulting in position-dependent frequency shifts in imaging with undesired IR signal variability. This problem is either addressed with a laser repetition rate sweep to find the maximum IR signal,[37] or more commonly by frequency tracking *via* a phase-locked loop (PLL).[2,21,38]

Here, we introduce force volume (FV) AFM-IR that is built upon the force volume AFM base mode, an established force spectroscopy technique.[39,40] It involves the collection of force−distance curves (here FV cycles) at each pixel of an image. Compared to RE AFM-IR, FV AFM-IR removes lateral forces and hence enables imaging and spectroscopy on fragile samples with sub-10 nm spatial resolution. When the laser is pulsing on resonance with a cantilever mode in resonance enhanced FV AFM-IR, or REFV, mechanical artifacts can be readily avoided with a phase-locked loop frequency tracking as in other AFM-IR modes. Inseparable from the FV cycle, nanomechanical data such as modulus or adhesion is obtained concurrently with IR data during probe retract segments, a characteristic shared with PFIR. Laser repetition rate sweeps can also be incorporated in FV AFM-IR. They create a three-dimensional data cube that contains valuable information about the contact resonance and Q-factor of a single chosen IR-driven cantilever mode (or multiple ones). Such frequency sweeps (FS) in FSFV AFM-IR represent an alternative to PLL frequency tracking similar to an implementation in RE AFM-IR.[37] Moreover, they allow to explicitly take the Q-factor of the detecting probe resonance into account in the IR sample response. Lastly, FV AFM-IR is also compatible with surface sensitive AFM-IR to limit the probing depth to a sample's top layer only.

RESULTS AND DISCUSSION

Implementation. The principle of FV AFM-IR is illustrated in Figure 1. The setup in Figure 1A follows the typical photothermal AFM-IR configuration, briefly explained here with more details in the method section. A wavelength- and repetition rate tunable infrared laser (IR laser) is focused on the tip−sample interaction region of an AFM probe using an off-axis parabolic mirror (OAP). The laser-induced photothermal AFM-IR signal is then sensed from changes in the vertical AFM beam bounce deflection using a lock-in amplifier.

Figures 1B-G illustrate a typical FV cycle, here executed with a nominally 0.2 N/m gold coated probe (Bruker, PR-UM-CnIR-B-10) on a PMMA domain of a PS-*b*-PMMA nanoparticle (sample is discussed later in more detail with respect to Figure 5). In FV a piezo actuator moves the tip toward the sample in a linear ramp motion at an adjustable speed (here: 27.3 μm/s, set as a frequency of 98 Hz) and from a defined ramp height (or size, in this example 140 nm) above the sample. This is illustrated by the height sensor data of Figure 1B for the first 5 ms of a FV cycle. Figure 1C depicts a force curve, *i.e.* probe deflection as a function of time, which can be translated into the typical force−distance curve of force spectroscopy[39,40] with the concurrently obtained height sensor data. At 4 ms in Figure 1C the tip snaps into contact with the sample causing a short negative vertical deflection. The piezo continues to translate the tip which linearly increases the deflection and hence tip−sample force. The piezo motion stops when a controlled force is met, the user-adjustable trigger threshold of here 5 nN (shortly after 5 ms). Depending on probe and sample, the trigger force can be sub-nN and is not defined as an absolute value but rather a relative one. That

https://doi.org/10.1021/acsnano.5c04015
ACS Nano 2025, 19, 18791−18803

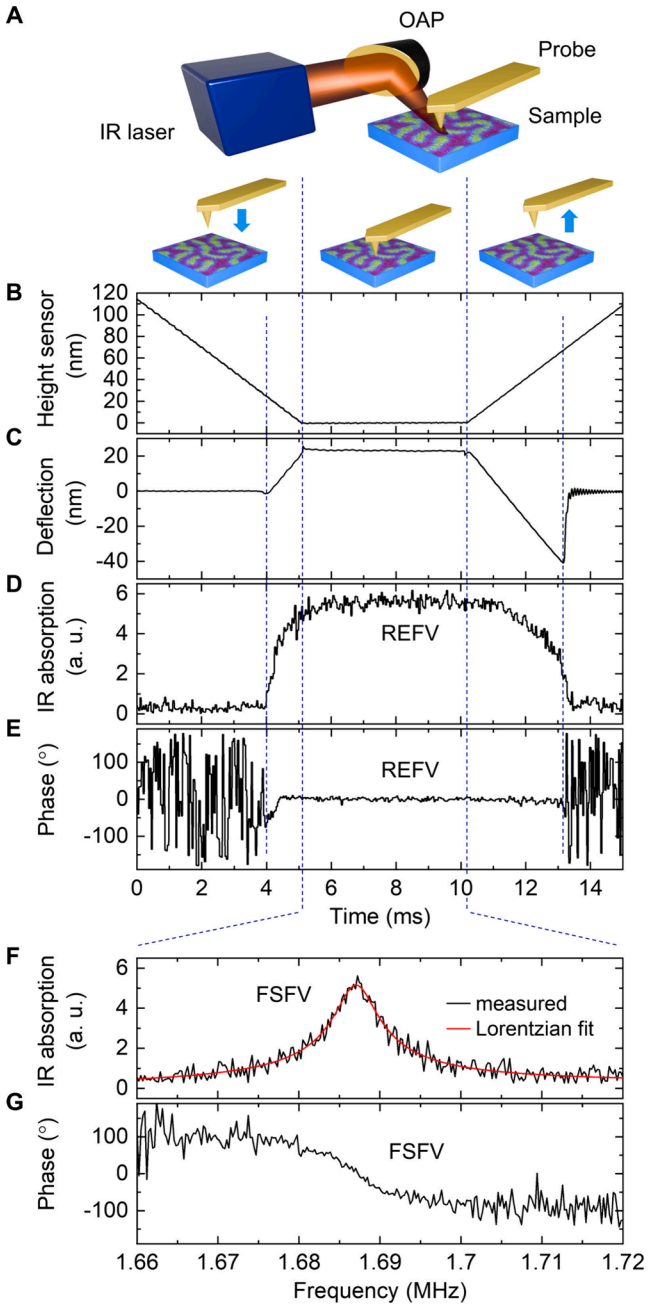

Figure 1. Principle of force volume (FV) AFM-IR. (A) Experimental setup with infrared light from an IR laser focused by an off-axis parabolic mirror (OAP) onto the tip−sample interaction region under the AFM probe. (B) Height sensor data as a function of time for a single FV cycle with a sketch of the probe movement for approach, hold, and retract. (C) Corresponding probe deflection representing a force curve. (D) Nonzero IR absorption signal in arbitrary units (a.u.) during tip−sample contact time, here for laser pulsing at a cantilever resonance in resonance-enhanced FV AFM-IR (REFV). (E) Corresponding phase, maintained at zero by a PLL during tip−sample contact and indicating efficient resonance frequency tracking. (F) In a second important modality, frequency-sweep FV AFM-IR (FSFV), the laser repetition rate during the hold time (of here 5 ms) is linearly swept over at least one contact resonance. A Lorentzian line shape (red line) fits the measured data (black line). IR absorption can be obtained as the peak amplitude or integral over the line shape. (G) Corresponding phase during FSFV (the PLL is inactive in FSFV).

means the probe deflection background is dynamically subtracted so that deflection drifts inherent in the absolute trigger of contact mode are compensated for. During a defined hold segment of 5 ms in this illustration the feedback is active to keep the vertical deflection constant. After this hold segment, the piezo actuator retracts the tip at around 10 ms and at the adhesion point (at 13 ms) the tip snaps off the surface. Engage and retract portions of the force curve can be evaluated for nanomechanical property information, *e.g.* adhesion, modulus or sample deformation.[40]

The hold segment with its constant controlled force is however utilized to acquire chemical information at the nanoscale *via* the photothermal AFM-IR response of the sample. In the resonance enhanced FV AFM-IR variant, REFV, the infrared laser is pulsed at a contact resonance of the probe for signal enhancement. In this example a higher mode in the 1.7 MHz range is used, and nanoscale IR absorption data is collected analogous to resonance enhanced AFM-IR. Figure 1D shows the time-dependent REFV signal, the IR absorption as amplitude output of the lock-in amplifier, which is nonzero only during the tip−sample contact time. The REFV signal rises during the varying force between 4 and 5 ms, remains constant during the constant-force hold segment until it decreases while the probe is retracting from the surface after 10 ms. In this REFV implementation, a phase-locked loop (PLL) is active. PLL frequency tracking in AFM-IR is a common technique to track resonance shifts caused by local sample stiffness variations.[2,21,38] The PLL is set up such that in a first step with disabled PLL and at a stationary xy sample position the laser repetition rate is tuned to maximize the lock-in amplifier amplitude during the hold segment. This way, the condition of resonance enhancement is met with the laser repetition rate matching a probe contact resonance. At this frequency the lock-in amplifier phase is shifted to zero by adding a phase offset. The PLL is then enabled, maintaining this zero-phase set point by changing the laser repetition rate accordingly. While compensating for frequency shifts between sample positions, the PLL in REFV can also track contact resonance shifts during varying tip−sample forces. This is reflected in the lock-in amplifier phase output (Figure 1E) that is kept at zero degree after an initial short period between 4 and 4.5 ms that the PLL requires to settle once the tip−sample contact has been established.

A second important variant of FV AFM-IR, frequency-sweep FV or FSFV, is introduced in Figure 1F. Here, during the hold segment the laser repetition rate is linearly swept covering at least one contact resonance of the probe. Figure 1F presents an example where the laser repetition rate spans the 1.66−1.72 MHz range within the 5 ms hold time. The frequency sweep range is user-adjustable but stays constant between FV cycles. A future improvement may include to dynamically determine the contact resonance and center the sweep range accordingly. The measured IR absorption in Figure 1F (black curve) follows a Lorentzian line shape (red fit). In FSFV the PLL is disabled in order not to interfere with the intended frequency stepping. Consequently, the corresponding phase signal in Figure 1G varies with frequency and follows the expected shape of a Lorentz oscillator. More details concerning FSFV covering a single or multiple contact resonances are discussed later with respect to Figures 5 and 6.

Figure 1 presents a single FV AFM-IR cycle, either executed in REFV or FSFV. The entire cycle is repeated at every xy pixel of a scan in imaging while the nanoscale IR absorption of

https://doi.org/10.1021/acsnano.5c04015
ACS Nano 2025, 19, 18791−18803

interest is only collected during the hold segments on the surface. Note that the IR response is not evaluated during the engage and retract segments with their varying forces. In REFV, the IR absorption is averaged over the hold segment in each pixel, in the example of Figure 1D between 5 and 10 ms. In FSFV, the IR absorption may be represented by the peak amplitude of a Lorentzian fit as in Figure 1F (red curve), or by an integral over the measured or fitted line shape as detailed later with respect to Figure 5. When moving between pixels, purely vertical engage and retract motion in FV ensures the absence of lateral forces in contrast to contact mode. For instance, see SI Figure S1 for the effect of lateral forces on the tip lifetime, and SI Figure S2 for the impact of lateral forces on a sample. In imaging the hold times are typically 2−5 ms for REFV when using a PLL, and tens to hundreds of ms for a laser repetition rate sweep during the hold segment in FSFV (see later discussions regarding Figures 5 and 6). FSFV can be executed within even shorter times (*e.g.*, 2 ms) albeit at the expense of signal-to-noise ratio. Additionally, as shown in SI Figure S3 the contact resonance line shape may suffer from asymmetry and a frequency shift for the fastest sweeps, likely depending on the Q-factor of the probe. Room for improvement exists, *e.g.* with respect to probe parameters (frequency and Q-factor) but has not been fully explored yet. In contrast to these relatively short hold times during imaging, the hold time in point spectroscopy in FV AFM-IR lasts until the spectrum acquisition has finished (can be several seconds to 10s of seconds).

Unique to force volume, the forces, engage and retract speeds, and hold times within single FV cycles may be varied to create a well-defined sequence of multiple engage, hold and retract segments. This sequence may be repeated for each sampled pixel and can contain also negative or 'pulling' tip−sample forces, meaning a net-attractive tip−sample force. The 'pulling' force causes the probe to bend toward the sample from its equilibrium deflection (as measured when not contacting the sample). An example of such a sequence is displayed in SI Figure S4 and may be used for loading/unloading or pulling experiments, *e.g.* on single proteins or molecules,[41] concurrently investigating conformational and nanochemical changes. Note that a negative trigger force in each FV cycle[42] may also be maintained in IR imaging to create entire maps at 'pulling' tip−sample forces (see Figure S5 as an example for FV topography mapping without IR illumination). In order to trigger on a negative trigger force or force set point a strong attractive tip−sample force is required and a probe that is not too stiff. That way, during the engage segment where the piezo moves the tip toward the sample, the probe snaps into contact causing a large downward bending of the cantilever. The continued piezo movement decreases this bend until the desired negative force set point is reached. Without a strong attractive tip−sample force, or if the probe's spring constant is too high, the cantilever may not bend enough toward the sample (Figure 1C is such an example), preventing reliable triggering on a negative force set point.

AFM-IR Resolution and Sensitivity. We first benchmark the most important characteristics of an AFM-IR technique, IR spatial resolution and sensitivity. To address the spatial resolution we turn to the model system of a poly(styrene-*b*-methyl methacrylate) (PS-*b*-PMMA) block copolymer film of 30 nm thickness on a silicon substrate. A soft (nominally 0.5 N/m) Au-coated nitride cantilever (Bruker, PR-UM-FnIR-A-10) was driven around its 1300 kHz vertical resonance for REFV AFM-IR data collection. The 500 nm, 256 × 256 pixel image was taken within 13 min at a ramp size of 80 nm, ramp rate of 156 Hz (approach/retract speed of 25 μm/s), a 5 ms hold time and with active PLL frequency tracking. While the topography (height sensor) image in Figure 2A shows little

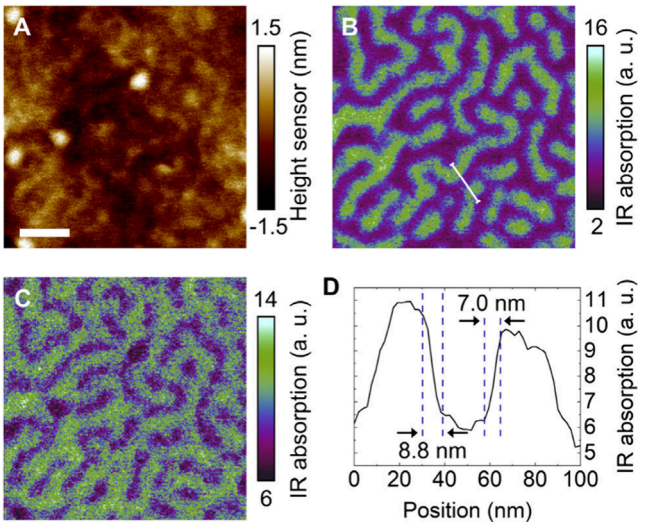

Figure 2. Sub-10 nm IR spatial resolution on a PS-*b*-PMMA block copolymer. (A) Topography of a PS-*b*-PMMA block copolymer film on silicon with a 100 nm scale bar. (B) IR absorption as measured with REFV AFM-IR at 1730 cm^{-1} corresponding to PMMA's carbonyl resonance. (C) IR absorption at 1492 cm^{-1}, associated with the aromatic ring stretch vibration of PS. (D) Line profile averaged across the 5-pixel wide line marked in (B), showing 7.0 nm IR resolution (defined at 90%−10% signal thresholds).

variation (below 3 nm), strong IR absorption is observed in panel B when probing the PMMA domain distribution at its characteristic 1730 cm^{-1} carbonyl resonance. The complementary PS domains are visualized at the 1492 cm^{-1} PS resonance in panel C, confirming the expected lamellae shaped domain arrangement with inverted contrast compared to panel B. An infrared spatial resolution of ∼ 7.0 nm is measured at the 90%−10% thresholds across the 5-pixel wide line cut marked in panel B. This is on par with tapping AFM-IR[19,20] and PFIR[35] on similar block copolymer films, and surpasses resonance enhanced contact mode with its <15−20 nm.[5,15,17] We speculate that the improved spatial resolution in REFV compared to RE AFM-IR is due to the absence of lateral forces. These forces cause tip and sample wear as well as tip contamination in contact mode based RE AFM-IR imaging. Additionally, in RE AFM-IR the tip may be dragged across the surface in a stick−slip motion due to friction from locally varying lateral forces. This way, a sample response may be associated with a new xy piezo position while the tip continues probing a previous position, leading to blurring of the IR and topography images.

While the 30 nm thin PS-*b*-PMMA sample already suggests high nanochemical sensitivity, we turn to a purple membrane model system to acquire REFV AFM-IR spectra on a monolayer sample. Note that the monolayer still consists internally of two phospholipid layers surrounding highly ordered crystals of bacteriorhodopsin protein. Imaging data at 128 × 128 pixels in Figure 3 has been recorded within 3 min

https://doi.org/10.1021/acsnano.5c04015
ACS Nano 2025, 19, 18791−18803

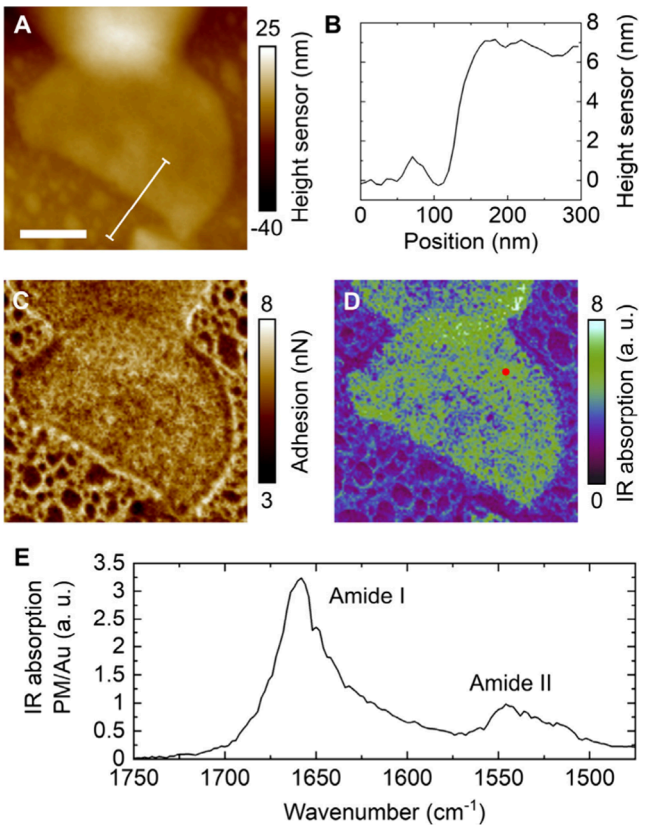

Figure 3. Purple membrane monolayer sensitivity. (A) Topography of the purple membrane on a gold substrate with 200 nm scale bar. (B) The purple membrane monolayer appears 7 nm thin across the line profile in (A). (C) Adhesion measured concurrently with topography. (D) IR absorption image at the 1660 cm^{-1} amide I band. (E) Monolayer point spectrum with amide I and II bands, obtained at the red marked location in (D).

using the previous 0.5 N/m nitride cantilever. A reduced 3 ms hold time was applied with active PLL, a 195 Hz ramp rate and 100 nm ramp size (approach/retract speed 39.1 μm/s). The monolayer deposited on a template-stripped gold substrate can be identified as the half-moon shape film in topography (Figure 3A) with its 7 nm step height measured across its edge in a line cut (panel B).[43] The simultaneously acquired adhesion in panel C as the minimum in the retract segment of the force curve reveals contrast between the smooth monolayer and the rougher gold substrate. IR absorption mapping (panel D) concurrently obtained during the FV hold segment at the amide I band at 1660 cm^{-1} further localizes the monolayer membrane protein. In Figure 3E a point spectrum displays the characteristic amide I and II bands. The nano spectroscopy and imaging data reproduce earlier measurements acquired in resonance enhanced AFM-IR.[43] The spectrum is presented as purple membrane REFV AFM-IR response divided by the nonvanishing gold substrate one, with offset removed (see SI Figure S6 for individual REFV AFM-IR spectra of the purple membrane and the gold substrate). Given a combined acquisition time for both membrane and substrate spectra of below 30 s the data emphasizes good sensitivity of the technique down to monolayer systems.

Correlative Quantitative Nanomechanical Imaging. Originating from the force volume operational AFM mode, FV AFM-IR inherently provides a full force−distance curve in each pixel. As in force spectroscopy or peak force tapping the retract curve of a FV cycle is fitted in real time to established mechanical models to obtain the local sample modulus and other local properties. As a demonstration of combined nanomechanical and nanochemical imaging, a spin-cast film of PS-LDPE (polystyrene − low-density polyethylene) is probed in Figure 4 with a cantilever of nominally 40 N/m spring constant (Bruker, PR-UM-TnIR-D-10). This cantilever is selected based on its stiffness and tip radius to allow high-performance nanomechanical probing in the expected sample modulus range. Because it is substantially stiffer than

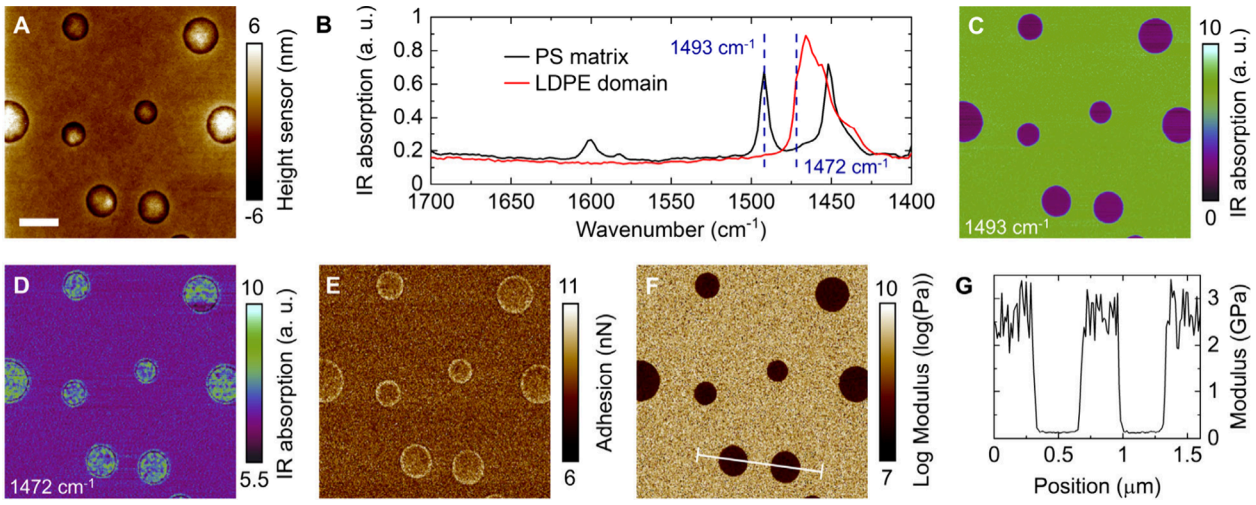

Figure 4. Correlative nanochemical and nanomechanical mapping on a PS-LDPE blend. (A) Topography of a PS-LDPE blend with a 500 nm scale bar. (B) Point spectroscopy in REFV AFM-IR on the PS matrix (black line) and on one of the LDPE domains (red line) with characteristic PS and LDPE resonances. Vertical dashed lines mark the wavenumbers used in subsequent IR absorption mapping at 1493 cm^{-1} and 1472 cm^{-1}, respectively. (C) IR absorption imaging at 1493 cm^{-1}, the aromatic ring stretch vibration of PS. (D) IR absorption mapping at 1472 cm^{-1} close to LDPE's CH_2 scissoring vibration. (E) Adhesion and (F) log modulus data simultaneously acquired with the IR maps. (G) Line profile from the modulus map, averaged over the corresponding area marked in (F). It illustrates quantitative modulus probing over more than an order of magnitude.

https://doi.org/10.1021/acsnano.5c04015
ACS Nano 2025, 19, 18791−18803

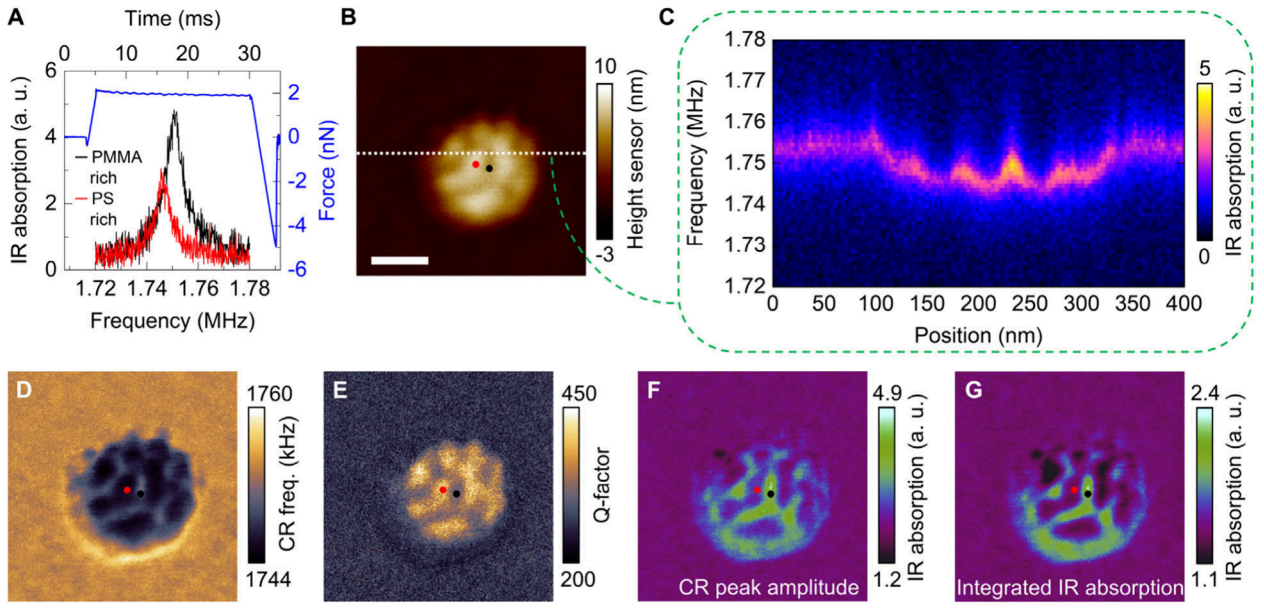

Figure 5. Frequency sweep FV AFM-IR (FSFV) on a PS-*b*-PMMA nanoparticle. (A) Laser repetition rate sweep across a single contact resonance during the 25 ms long FV hold time (see blue force curve). The two highlighted locations are indicated by the black and red dots in the topography image in (B) with a 100 nm scale bar. PMMA rich (black curve) and PS rich (red curve) areas of the PS-*b*-PMMA nanoparticle reveal a contact resonance around 1.75 MHz. The wavenumber was chosen to match PMMA's carbonyl resonance (1730 cm^{-1}). (C) Contour plot of the frequency sweep at each position along the white dotted line in (B). (D) Contact resonance (CR) frequency obtained from Lorentzian fits of the frequency sweeps in each pixel of the image. (E) Corresponding Q-factor extracted from Lorentzian fits. (F) CR peak amplitude from Lorentzian fits representing IR absorption at 1730 cm^{-1}. (G) Integrated IR absorption over the frequency sweeps from 1720 to 1780 kHz.

aforementioned probes, a small ramp size of 40 nm (at 98 Hz ramp rate or approach/retract speed of 7.8 μm/s) is sufficient to overcome the adhesion force in each FV cycle without intermittently sticking to the surface. Circular domains of LDPE observed in the topography image in Figure 4A show distinct peaks in point spectroscopy (Figure 4B, red curve) compared to the surrounding PS matrix (black curve). IR absorption mapping at the PS resonance of 1493 cm^{-1} confirms uniform PS distribution in the matrix in Figure 4C. In panel D, the IR contrast is reversed for IR absorption mapping at the 1472 cm^{-1} LDPE resonance. The LDPE domains reveal an internal structure in the nanochemical image (panel D). Note that a PLL was active to follow any contact resonance frequency shift during IR mapping. The ring structure around the LDPE domains in the LDPE absorption of panel D has no correspondence in the PS absorption map of panel C. The dark ring of diminished absorption overlaps with a spike in adhesion (panel E) and a dip in topography at the PS-LDPE interface (see SI Figure S7 for more details). We speculate that heat diffusion from LDPE into the surrounding PS matrix might contribute to this absorptive ring structure at the LDPE absorption peak. Another factor might be the expected variations in the Q-factor and hence IR absorption signal scaling at the interface between these soft (LDPE) and hard (PS) sample components. A detailed analysis in terms of nanochemical contrast of this interesting soft–hard model system is left for the future.

Concurrently with IR imaging, nanomechanical data is extracted in panel E (adhesion) and panel F (log modulus). For quantitative measurements, the standard procedure of relative calibration on a known modulus sample was followed. The result is illustrated in panel G as a line cut in the modulus map across the two LDPE domains specified in panel F. The measured modulus values of 130 MPa and 2.7 GPa for LDPE and PS, respectively, fall within the expected range for these polymers.[33] Note that the calculated PS modulus exhibits higher noise due to low indentation of the probe into the stiff PS matrix which leads to inaccuracy in the fitting of the nanomechanical model. Nevertheless, the compatibility with low and high spring constant probes grants FV AFM-IR access to nanomechanical properties over a large modulus range. This has been demonstrated here for a relatively stiff cantilever still delivering quantitative data over the 100 MPa to 3 GPa range.

We would like to briefly address similarities and differences between nanochemical and nanomechanical mapping. Probing solely the mechanical properties, *e.g.* the modulus, without IR illumination reveals a similar contrast between domains as in the nanochemical images of Figures 4C and D (for PS-LDPE) or Figures 2B and C (for PS-*b*-PMMA). Examples are given in Figures 4E and F (for PS-LDPE), or by the modulus mapping in PFIR[35] for a PS-*b*-PMMA sample. Hence, for such simple two-phase systems of known constituents the phases can be discerned based on their mechanical properties. That approach often breaks down for real-world three- (and more) component systems, even if the phases are known. The moduli of the components may lie close together as is the case for many polymers,[33] and the uncertainty in determining these values in nanomechanical measurements may be substantial.[33] Furthermore, the properties of domains in a composite may differ from the bulk due to confinement, mixing and phase changes of the constituent materials during sample preparation.[44] Consequently, a contrast in nanomechanical properties might not be measurable and/or cannot be used to identify phases unambiguously. In the case of unknown sample constituents, it is mostly impossible to make a phase assignment based on the limited set of nanomechanical data.

https://doi.org/10.1021/acsnano.5c04015
ACS Nano 2025, 19, 18791–18803

In contrast, infrared spectra of materials including polymers are uniquely different in the 'fingerprint' region and thus allow a faster, much more convenient and accurate way to discern materials at the nanoscale. IR mapping at select wavelengths can then accurately highlight chemical distributions whereas a nanomechanical contrast might be lacking or cannot be assigned to phases.

Frequency Sweep over a Single Probe Resonance. While aforementioned data were recorded at a single laser repetition rate with activated PLL for frequency tracking (REFV implementation), we now turn to an alternative in the form of frequency sweep force volume AFM-IR (FSFV AFM-IR). This variant has been briefly introduced in Figures 1F and G. It provides additional sample information (specifically local contact resonance frequency and Q-factor) and presents an interesting alternative to PLL-based frequency tracking. To this end, as illustrated in Figure 5A, the laser repetition rate during a hold segment is swept, here from 1720 kHz to 1780 kHz for each pixel in an image (black and red resonance curves in Figure 5A for the two different sample domains). To accommodate the frequency sweep a 25 ms long hold time was selected as exemplified by the blue force curve, that is the deflection (similar to Figure 1C) multiplied by the probe's calibrated 0.09 N/m spring constant. The chosen sweep duration of 25 ms does not alter the contact resonance line shape (see SI Figure S3) while delivering good signal-to-noise ratio at reasonable measurement speeds. As a sample we introduce a PS-*b*-PMMA block copolymer on a silicon substrate that forms small nanoparticles with PS and PMMA rich domains. Their small size and fragility render them very challenging or impossible to investigate in contact mode based RE AFM-IR while they prove suitable for FV AFM-IR (see SI Figure S2 for an imaging comparison on these nanoparticles). The topography of such a PS-*b*-PMMA nanoparticle obtained in FSFV is presented in the 256 × 256 pixel map of Figure 5B. The chosen frequency sweep range of 1720−1780 kHz overlaps with a contact resonance of the nominally 0.2 N/m cantilever (Bruker, PR-UM-CnIR-B-10) so that a Lorentzian shaped contact resonance curve of IR absorption is associated with each image pixel. The wavenumber 1730 cm^{-1} was selected to match the characteristic carbonyl resonance of the PMMA constituent. The displayed black and red curves in Figure 5A stem from the black and red marked locations in Figure 5B, the PMMA rich and PS rich domains of the nanoparticle, respectively. An IR absorption signal decrease is observed for the red marked area (PS dominates) compared to the black marked location (PMMA dominates). Figure 5C represents the variation of the contact resonance frequency across the entire horizontal dotted white line in Figure 5B. It shows ∼ 10 kHz shifts between the silicon substrate and the different regions of the nanoparticle. In common contact resonance AFM modalities,[45] changes in cantilever resonant behavior are used to detect variations in mechanical properties across the sample. In particular, when the cantilever is mechanically excited this is referred to as ultrasonic atomic force microscopy (UAFM) while atomic force acoustic microscopy (AFAM) involves mechanical excitation of the sample. In either case, elastic and viscoelastic sample properties can be calculated from the contact resonance (CR) spectra,[46−49] including in force volume operation.[50] In our work photothermal excitation replaces the mechanical actuator to cause a sample surface oscillation, representing an alternative route to acquire AFAM contact resonance data. Such an IR absorption-based excitation of the contact resonance provides a few benefits, *e.g.* operation does not require a sample actuator and hence can be applied to any IR absorbing sample. Furthermore, the CR frequency does not need to be matched to the actuator. A weakness of this method is that the extracted elastic/viscoelastic properties may be affected by the concurrent local sample heating effectuated by IR absorption. This is especially true for samples that have phase transitions near the measurement temperature.

Since every pixel contains a frequency sweep across the 1750 kHz contact resonance, Lorentzian line shape fitting is a useful way to parametrize the contact resonance. It allows qualitative inference of mechanical sample properties, for instance the local contact resonance center frequency in Figure 5D. Note that Lorentzian fitting of the contact resonance curves is only an approximation for the line shape of a driven, damped harmonic oscillator that the photothermally actuated probe presents. The PS rich areas exhibit a reduction in frequency compared to the PMMA domains, which is expected from their different modulus of ∼ 3.1 GPa for PMMA and ∼ 2.7 GPa for PS.[30] The Q-factor in Figure 5E represents another meaningful contact resonance fit parameter that associates the PS rich regions with a 50% larger Q-factor than the PMMA rich ones. An increased contact resonance Q-factor is an indication of decreased internal dissipation or loss tangent. In this case, the Q-factor is anticorrelated with the adhesion: the PMMA rich domains exhibiting lower Q-factors and hence higher internal damping are associated with an increased adhesion. This suggests a link between adhesion and internal damping in these materials (see SI Figure S8 for the corresponding adhesion map). Further CR-based analysis (following for example reference[45]) would allow quantification of sample storage and loss modulus (and loss tangent) at the CR frequency. Access to these properties is granted in FSFV AFM-IR in addition to those following directly from the force curve (*e.g.*, low frequency modulus or adhesion).

Nanochemical mapping is displayed in Figure 5F where the peak amplitude of the Lorentzian fits is extracted as CR peak amplitude. At the chosen wavenumber of 1730 cm^{-1} matching the PMMA carbonyl absorption, Figure 5F displays the PMMA distribution of the nanoparticle. Note that the nonzero signal in PS rich regions at a nonabsorbing wavelength (1730 cm^{-1}) for PS may mainly be attributed to a nonzero substrate response of comparable magnitude and to a minor extent to an ill-defined interface between PS and PMMA domains. The shown quantity in Figure 5F of peak amplitude of the Lorentzian line shape fits is basically identical to typical AFM-IR imaging at a single laser repetition rate under active PLL frequency tracking: in this case the PLL follows the IR signal, usually the maximum, that is the resonance peak. This is qualitatively confirmed in SI Figure S9 for the FV AFM-IR experiment but now executed in the REFV modality with active PLL instead of the frequency sweep implementation. Note that the IR absorption contrast in Figure 5F (or equivalently in SI Figure S9A for REFV at a single laser repetition rate and enabled PLL) requires to follow the contact resonance. Reading the IR absorption signal at a fixed laser repetition rate without frequency tracking may result in IR contrast inversion between the PS and PMMA rich domains leading to ambiguous domain assignments. This is exemplified in SI Figure S10 where the IR absorption data acquired with FSFV AFM-IR was evaluated at different constant frequencies covered by the sweep. This underlines the importance of PLL

https://doi.org/10.1021/acsnano.5c04015
ACS Nano 2025, 19, 18791−18803

tracking, or the benefit of recording the full resonance sweep in FSFV AFM-IR.

Having access to the contact resonance line shape in IR absorption, specifically its width as Q-factor or full-width at half-maximum $fwhm$ ($fwhm = f_0/Q$) at resonance frequency f_0, offers an important benefit: mechanical damping of the IR response of the sample can be taken into account. This is not supported in the current benchmark AFM-IR techniques of tapping AFM-IR, resonance enhanced AFM-IR, surface sensitive AFM-IR and PFIR. Conventionally, a peak amplitude of the contact resonance, or a value close to it, is recorded. Ideally a frequency tracking mechanism such as a PLL is employed to ensure that the peak amplitude is measured irrespective of mechanical variations at the probed locations. Although frequency shifts due to contact stiffness are compensated this way, the Q-factor of the resonance, *i.e.* the damping, is not considered. The amplitude at a fixed frequency usually measured with a Lock-In amplifier analyzing the vertical deflection is proportional to the sample's thermal expansion. The latter is in turn proportional to the sample's absorbance. When operating on or near resonance, the amplitude depends on both the absorbance and the Q of the resonance (variations arising from mechanical damping in the tip−sample contact area). Averaging over all frequencies across a contact resonance is then also proportional to the sample's absorbance but now includes the contact resonance line shape, *i.e.* the damping. It is thus a more accurate representation of the IR absorption. Such averaging or integration (equivalent except for a constant factor of the integration length) can be routinely performed on the FSFV AFM-IR contact resonance sweep data. Presented in Figure 5G, the integrated signal over the 1720−1780 kHz sweep range (or correspondingly over the entire 25 ms long hold time here) resembles the IR absorption deduced from the peak amplitude in Figure 5F. Differences are visible though in a higher contrast between the IR absorption signal on the PS rich domains (red dot) compared to the PMMA domains (black dot). The signal on the PS rich areas is on par or below the response on the silicon substrate for the integrated signal in Figure 5G, whereas it is larger than the substrate when recording the peak amplitude in Figure 5F. The integral over a Lorentzian line shape is the peak amplitude times the $fwhm = f_0/Q$. In other words the integrated IR absorption in Figure 5G is proportional to peak amplitude over Q-factor. A 50% higher Q-factor on the PS rich domains (compared to the PMMA rich structures) as indicated in Figure 5E implies that the integrated IR signal on the PS domains (Figure 5G) is comparatively lower than the CR peak amplitude value (Figure 5F). The resonance center frequency f_0 remains mostly constant, the change is below 1% in Figure 5D. Hence, the Q-factor variation represents the most significant mechanical property change between the domains. Note that the dissimilarity in modulus between PS and PMMA (~2.7 GPa vs ~ 3.1 GPa, respectively) is minor. Therefore, more heterogeneous material systems are expected to show larger differences between IR absorption from single frequency data compared to integrating (or averaging) over frequency sweeps.

Frequency Sweep over Multiple Probe Resonances. Usually the IR absorption in AFM-IR is evaluated at a single cantilever resonance as in the previous section. However, FSFV AFM-IR allows to probe multiple resonances during each hold segment and in each pixel of an image. An example of such a frequency sweep of the laser repetition rate is depicted in Figure 6A. It covers 100−2100 kHz in a 1 s long hold segment in FSFV AFM-IR (here averaged over 10 different pixels). A

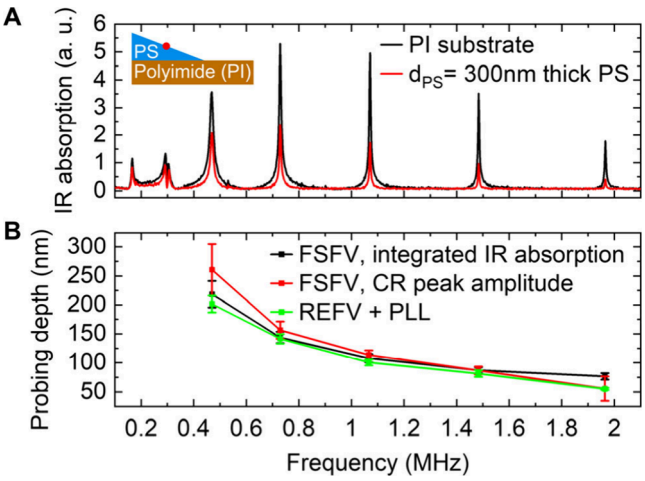

Figure 6. Multiresonance frequency sweep in the FSFV implementation on a PS wedge on a polyimide (PI) substrate. (A) Example of two frequency sweeps covering several contact resonances of a PR-UM-CnIR-B-10 cantilever on a 25 μm thick polyimide (PI) film (black curve) and a d_{PS} = 300 nm thick polystyrene (PS) area on top (red curve). The 1720 cm^{-1} polyimide absorption is probed over the 100−2100 kHz range. The inset depicts a sketch of the sample, a PS wedge on a PI film. The red dot exemplifies a location to probe at a defined PS layer thickness, *e.g.*, at d_{PS} = 300 nm. The sweep illustrates that different modes exhibit different relative signal strengths (on PI versus PS) based on their probing depth. (B) Extracted probing depths at five of the seven contact resonances from (A). They are obtained from the 1720 cm^{-1} polyimide IR absorption imaging of the sample. Three different methods are compared: integrating the frequency sweep data over the contact resonance, fitting the contact resonance with a Lorentzian fit to extract the CR peak amplitude, and measuring the amplitude directly at a fixed frequency in REFV (without a frequency sweep but with PLL tracking). Error bars represent the error in fitting the exponential decay law. The results match for all three methods within error bars.

nominally 0.2 N/m cantilever (Bruker, PR-UM-CnIR-B-10) was used to create a 64 × 16 pixel map (8 × 2 μm size) of a PS wedge on a polyimide film (25 μm thick commercial kapton tape). The scan area is the intersection where both constituents are exposed (see sketch in Figure 6A). The 1720 cm^{-1} polyimide absorption band was probed for the laser repetition rate dependent IR absorption. The black curve in Figure 6A has been acquired on the polyimide substrate and the red curve is associated with a PS location on the wedge with a local PS thickness of d_{PS} = 300 nm. It is known that the probing depth in resonance enhanced AFM-IR is frequency dependent with increased surface sensitivity for higher laser repetition rates,[2,30,51−53] mainly attributed to a smaller thermal diffusion length. Consequently, probing the IR absorption in a frequency sweep covering several resonances simultaneously means concurrent detection at different probing depths, so that in the best case the thickness of surface layers may be reconstructed.[30]

Next, we look into the probing depths of the individual cantilever modes in more detail. To this end we follow the previously outlined procedure.[2,30] We use the position and laser repetition rate dependent IR absorption (exemplified in Figure 6A) across the sample region where the PS wedge thins

https://doi.org/10.1021/acsnano.5c04015
ACS Nano 2025, 19, 18791−18803

and vanishes to expose the underlying polyimide substrate. The simultaneously acquired topography image allows us to correlate for each image pixel the local PS thickness with the measured IR absorption (at the 1720 cm^{-1} polyimide band). We arrive at a PS-thickness dependent IR absorption (see SI Figure S11 for more details). We compare three different acquisition methods. In the first method, for each contact resonance separately the IR absorption is calculated from the 100−2100 kHz frequency sweep as the integral over a 100 kHz wide window around the respective resonance. The second approach utilizes a Lorentzian line shape fit of the individual contact resonances to obtain the CR peak amplitude as IR absorption signal. Lastly, we compare to the IR absorption acquired in REFV: we image the PS wedge sample at a single laser repetition rate set to an individual contact resonance that is tracked with a PLL. This latter method represents the acquisition procedure underlying the IR maps in Figures 2-4. For a single contact resonance, and for all three measurement routines the extracted IR absorption signal $A(d_{PS})$ as a function of PS thickness d_{PS} can be well fitted to an exponential decay law[30] with fit parameters $m_{1,2,3}$:

$$A(d_{PS}) = m_1 + m_2(1 - e^{-d_{PS}/m_3}) \quad (1)$$

The exponential decay constant m_3 may be interpreted as probing depth.[30] That means m_3 represents the top layer thickness (here PS) at which the IR absorption signal has reached $(1\text{-}e^{-1})$ = 63% of its maximum for an infinitely thick top layer (above an offset m_1). Results of the probing depths for five resonances in the 100−2100 kHz sweep window are shown in Figure 6B for the three described methods to assess the IR absorption from the FV AFM-IR data across the PS wedge. The general trend of a smaller probing depth with higher frequencies is well confirmed.[2,30,51−53] Furthermore, all three methods to extract IR absorption match reasonably well within error bars. At the 1965 kHz mode the results deviate more since the signal strength on PS and hence the signal-to-noise ratio is smaller than at lower-frequency modes due to the reduced probing depth (see SI Figure S11). Additionally, the smaller probing depth means that fitting results rely to a larger extend on the thin PS region of the wedge, an interface area of the two material components that is less well-defined. In the analysis this is partially accounted for by excluding the first 10 nm of PS thickness in the exponential decay fitting in general. On the low-frequency side of the resonances, the 470 kHz mode data also exhibit a larger variation. This is likely due to the probing depth fit parameter m_3 approaching the maximum evaluated PS thickness of d_{PS} = 640 nm, rendering fitting less accurate (see SI Figure S11). Note that the ∼300 kHz and ∼170 kHz modes have not been evaluated: the ∼300 kHz mode consists of two overlapping vertical and horizontal cantilever resonances, and the signal-to-noise ratio of the ∼170 kHz mode is poor since the large probing depth renders the mode rather insensitive to the PS presence.

We remark that access to the AFM-IR responses at different cantilever resonances allows a tomography-like reconstruction of embedded objects. Dazzi *et al.*[30] reconstructed the shape of a surface object within a matrix. More complicated cases, specifically subsurface components within another phase, seem feasible. From the AFM-IR signal of a single probe resonance one cannot discriminate yet with current methods a thin absorber near the surface from a thick absorber of the same material but buried deeper. However, a different resonance probing for instance deeper would measure a larger signal by comparison for the same object depth. Hence, AFM-IR signal ratios between different resonance modes allow to infer a depth of the probed buried absorber while the absolute signal strength indicates its thickness. At least a calibration of the probing depth for each resonance is required as discussed above with respect to Figure 6B (or see Dazzi *et al.*[30]). Additionally, the decrease of lateral resolution with depth needs to be considered.[53] We speculate that the described concept together with the simultaneous acquisition of several resonance modes in FSFV AFM-IR can push AFM-IR based tomography into real-world applications beyond the current proof-of-concept studies.[30]

Surface Sensitivity. Having established the laser repetition rate dependent probing depth in FSFV AFM-IR, we attempt to visualize the impact for a wavelength-dependent IR absorption spectrum at various PS thicknesses d_{PS} of the same PS wedge on the polyimide film substrate. The black dotted curve in Figure 7 is a spectrum acquired in REFV at a position where

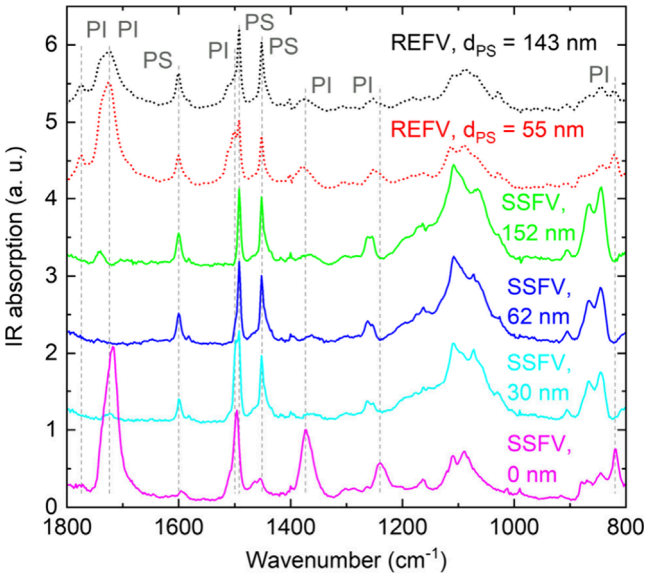

Figure 7. Surface sensitive probing on a PS wedge on a polyimide (PI) substrate. Comparison of the IR absorption spectra for PS of different thicknesses d_{PS} on the polyimide film (at the 1482 kHz contact resonance from Figure 6A). REFV (dotted lines) is contrasted with surface sensitive (SS) FV AFM-IR (solid lines). For the latter the cantilever was mechanically modulated at 3087 kHz and the IR amplitude was detected at the same 1484 kHz resonance (slightly shifted) but now with the laser pulsing at the difference frequency of 1603 kHz. Vertical dashed lines mark the most dominant PS or PI absorption lines, respectively. Spectra are vertically offset for clarity and REFV spectra are scaled (/3). While REFV probes through the PS top layer into the PI substrate, SSFV spectra only reveal the PS top layer.

the PS wedge is d_{PS} = 143 nm thick. To achieve a high surface sensitivity, the IR detection mode at 1482 kHz has been chosen. According to Figure 6B this mode is associated with a probing depth of $m_3 \approx 85$ nm, *i.e.* the IR absorption of a d_{PS} = 85 nm thin top layer would account for 63% of the IR absorption signal for an infinitely thick layer of that material. The displayed d_{PS} = 143 nm thin PS film (black curve) would accordingly represent 81% of the maximum IR signal with little contribution from below (if the substrate material was uniformly PS). The distinct PS absorption peaks at 1601 cm^{-1}, 1493 cm^{-1} and 1452 cm^{-1} are clearly identified,

https://doi.org/10.1021/acsnano.5c04015
ACS Nano 2025, 19, 18791−18803

however, the polyimide bands at 1773 cm^{-1}, 1729 cm^{-1} and to a smaller extend 1504 cm^{-1} and 820 cm^{-1} are also present. Probing a thinner d_{PS} = 55 nm PS film location (red dotted curve) samples deeper into the PI substrate and hence increases the absorption bands characteristic to PI. This renders it more difficult to distinguish the top layer PS absorption from the underlying polyimide substrate.

In order to enhance the surface sensitivity, we may either further increase the laser repetition rate (which is currently limited by the available laser technology and the AFM deflection laser detector bandwidth), or resort to the heterodyne detection scheme of surface sensitive AFM-IR[2] that can be implemented in FV AFM-IR operation. To this end a piezo actuator drives a higher contact resonance in surface sensitive (SS) FV AFM-IR, here around 3087 kHz. The laser is pulsing at 1603 kHz and the IR detection occurs at the same, slightly shifted, 1484 kHz mode as before in REFV. The nonlinear detection process now results in a significantly lower probing depth. The PS film spectrum is not contaminated any more by polyimide substrate absorption bands for a comparable PS film thickness of d_{PS} = 152 nm and the only slightly increased laser repetition rate of 1603 kHz (green curve in Figure 7). Even when reducing the film thickness further to d_{PS} = 62 nm (blue curve) or d_{PS} = 30 nm (cyan curve), PS bands dominate the spectrum while polyimide absorption peaks at 1725 cm^{-1} and 1499 cm^{-1} start to emerge in SSFV AFM-IR (cyan curve, d_{PS} = 30 nm). For comparison, the spectrum on polyimide alone without any PS top layer (magenta curve, d_{PS} = 0 nm) confirms the absorption band assignments. The compatibility with the heterodyne detection scheme of surface sensitivity AFM-IR and hence the ability to probe only the top layer on an absorbing substrate represents an important benefit of FV AFM-IR. It might help to address new applications in areas sensitive to the lateral forces of the original contact mode based surface sensitive AFM-IR technique.

As a last point, we remark that FV AFM-IR should be well suited to operate in liquid. FV as base AFM mode has been applied to study mechanical properties of biological samples in that environment.[54] The resonance enhanced detection underlying REFV has been successful in fluid in PFIR[55] and resonance enhanced AFM-IR.[4] However, background signal from fluid absorption poses a challenge.[2] Heterodyne techniques separating the IR detection frequency from the IR modulation frequency are advantageous in this regard, as demonstrated for tapping AFM-IR in the aqueous environment.[2] We expect surface sensitive FV AFM-IR as another heterodyne technique to similarly suppress unwanted signal from liquid.

CONCLUSIONS

In conclusion, we introduced an AFM-IR variant based on force volume AFM operation. As a natural extension to resonance enhanced contact mode, FV AFM-IR overcomes some of its limitations. The vertical approach and retract movement between tip and sample ensures the absence of lateral forces in contrast to resonance enhanced or surface sensitive AFM-IR with its constant tip−sample contact. This allows access to fragile samples such as the discussed PS-*b*-PMMA nanoparticle while monolayer sensitivity is achievable together with an IR spatial resolution <10 nm.

Since FV AFM-IR is built upon force volume, an established force spectroscopy technique, quantitative nanomechanical sample information is concurrently extracted in each FV cycle, a trait shared only with PFIR. This also means precise force control and control over the relative tip−sample position. Such defined access to small tip−sample distances combined with measurement of the IR response may also shed more light on the origin of photoinduced tip−sample forces and help to distinguish short-range photothermal sample expansion as in AFM-IR from long-range dipole−dipole forces as in photoinduced force microscopy (PiFM).[20,23,56]

An important characteristic of FV AFM-IR is the ability to sweep the laser repetition rate during the hold time to record the IR response as an IR absorption contact resonance curve. From a nanomechanical point of view this provides the local contact resonance frequency and Q-factor. Moreover, the IR induced photothermal sample excitation presents an alternative to the conventional mechanical excitation of the sample or tip in contact resonance AFM.[45] It should be feasible to extract elastic and viscoelastic material properties with nanoscale spatial resolution, in addition to modulus or adhesion information from the force curve alone. From a nanochemical point of view, such frequency sweeps can be fitted to a Lorentzian line shape. The extracted peak amplitude was shown to serve as an IR absorption signal. This is then analogous to conventional AFM-IR data acquisition obtained with a PLL to remove the effect of mechanically induced shifts in the resonance frequency of the probe. Such frequency sweeps in FV AFM-IR may prove a valuable option in cases where a PLL based frequency tracking approach runs into limitations, *e.g.* on inhomogeneous samples with large contact resonance frequency variations.

Importantly, such sweeps over a contact resonance can also take into account the Q-factor and hence mechanical damping in the IR response to reveal the 'true' nanoscale IR absorption. Conventional AFM-IR techniques only record the peak amplitude and would not capture the resonance line width or Q-factor and hence cannot compensate for changes in damping. Using a PS-*b*-PMMA nanoparticle as an example, accounting for damping by integrating over the contact resonance already showed a higher contrast in the IR absorption between PS and PMMA (due to a 50% difference in Q-factor) compared to looking at the peak amplitude alone. Furthermore, the repetition rate sweep range can be extended to comprise multiple contact resonances. This proved valuable for collecting IR responses at different probing depths which can serve to reconstruct a vertical material composition in a tomography-like manner.[30]

Lastly, borrowing the IR signal detection principle from RE AFM-IR, REFV AFM-IR can benefit directly from improvements to RE AFM-IR. In that regard, implementation of surface sensitive detection has been demonstrated here. Other innovative refinements such as the null-deflection approach based on a piezo-driven sample[16] appear feasible, as well as operation in fluid.

In summary, FV AFM-IR combines the sensitivity of resonance enhanced AFM-IR with the resolution of tapping AFM-IR. It adds force control, nanomechanical information, the ability to incorporate surface sensitive probing and importantly the ability to conduct laser repetition rate sweeps to measure single or multiple contact resonance curves and thereby integrate damping into the IR response. These characteristics should establish FV AFM-IR as a valuable addition to the existing suite of AFM-IR techniques.

https://doi.org/10.1021/acsnano.5c04015
ACS Nano 2025, 19, 18791−18803

MATERIALS AND METHODS

Sample Preparation. *Purple Membrane.* A solution of purple membrane flakes in deionized water of 5 μg/mL was drop cast on a template-stripped gold substrate and air-dried.

PS-LDPE. The PS-LDPE sample, spin-cast on silicon substrate, with LDPE domains within a PS matrix is from Bruker (P/N: PS-LDPE-12M).

PS-b-PMMA. A 1% (wt) solution of poly(styrene-*b*-methyl methacrylate) (PS-*b*-PMMA, Polymer Source Inc. P719-SMMA, M_n(PS) = 72.6 kg/mol and M_n(PMMA) = 70.9 kg/mol, M_w/M_n = 1.09) was prepared in propylene glycol monomethyl ether acetate (PGMEA, Sigma-Aldrich P/N 484431). The solution was spin coated on a small silicon substrate and annealed for 5 min at 200 °C.

PS-b-PMMA Nanoparticles. A 3 μg/mL solution of poly(styrene-*b*-methyl methacrylate) (PS-*b*-PMMA, Polymer Source Inc. P8537-SMMA, M_n(PS) = 95 kg/mol and M_n(PMMA) = 92 kg/mol, M_w/M_n = 1.10) was prepared in propylene glycol monomethyl ether acetate (PGMEA, Sigma-Aldrich P/N 484431). The solution was spin coated on a small silicon substrate and air-dried.

PS Wedge on Polyimide. A 3% (wt) solution of polystyrene (Polymer Source Inc. P471−S, M_n = 70.4 kg/mol, M_w/M_n = 1.04) was prepared in propylene glycol monomethyl ether acetate (PGMEA, Sigma-Aldrich P/N 484431) and drop casted on kapton tape (Bertech KPT-1). Subsequent evaporation was assisted *via* nitrogen gas flow.

AFM-IR Setup and Probes. FV AFM-IR was implemented on a Dimension IconIR system from Bruker equipped with an infrared tunable QCL (MIRcat) from DRS Daylight Solutions. Other lasers such as OPOs covering different wavelength ranges are compatible as well with this AFM-IR mode and instrument. The IR light is focused on the tip−sample interaction region and polarized along the AFM tip. The light source repetition rate is either modulated at a cantilever resonance in REFV or swept over a defined frequency range in FSFV. The resulting sample response is demodulated from the vertical cantilever deflection using a built-in Lock-In amplifier. The laser pulse length was fixed at 100 ns. Atmospheric water absorption was reduced by dry air purging of the instrument. Different cantilevers from Bruker with overall gold-coating were employed covering a wide stiffness range of nominally 0.2 N/m (PR-UM-CnIR-B-10), 0.5 N/m (PR-UM-FnIR-A-10), 5 N/m (PR-UM-PFIR-A-10), and 40 N/m (PR-UM-TnIR-D-10). The presented methods are also applicable to alternative probe models.

ASSOCIATED CONTENT

Data Availability Statement

The raw data used in this study are openly available on Zenodo at https://doi.org/10.5281/zenodo.15326265.

Supporting Information

The Supporting Information is available free of charge at https://pubs.acs.org/doi/10.1021/acsnano.5c04015.

> Imaging quality comparison between force volume (FV) and resonance-enhanced (RE) AFM-IR; contact resonance curves for different hold times; sequence of hold segments with positive and negative force set points in FV AFM-IR; FV AFM-IR topography mapping at negative force set points; REFV AFM-IR spectra of purple membrane and its gold substrate; details on the ring structure in the REFV AFM-IR absorption image of LDPE domains; adhesion and Q-factor across a PS-*b*-PMMA nanoparticle; comparison of the two IR imaging acquisition methods of REFV and FSFV AFM-IR; IR absorption contrast in frequency sweep FV AFM-IR data for fixed frequency readout; procedure to determine the probing depth on a PS wedge (PDF)

AUTHOR INFORMATION

Corresponding Author

Martin Wagner − *Bruker Nano Surfaces Division, Santa Barbara, California 93117, United States;* orcid.org/0009-0002-7432-4940; Email: martin.wagner@bruker.com

Authors

Qichi Hu − *Bruker Nano Surfaces Division, Santa Barbara, California 93117, United States*

Shuiqing Hu − *Bruker Nano Surfaces Division, Santa Barbara, California 93117, United States*

Cassandra Phillips − *Bruker Nano Surfaces Division, Santa Barbara, California 93117, United States*

Weijie Wang − *Bruker Nano Surfaces Division, Santa Barbara, California 93117, United States*

Bede Pittenger − *Bruker Nano Surfaces Division, Santa Barbara, California 93117, United States;* orcid.org/0000-0002-5980-878X

Alireza Fali − *Bruker Nano Surfaces Division, Santa Barbara, California 93117, United States*

Chunzeng Li − *Bruker Nano Surfaces Division, Santa Barbara, California 93117, United States*

Jérémie Mathurin − *Institut de Chimie Physique, Université Paris-Saclay - CNRS, 91400 Orsay, France*

Alexandre Dazzi − *Institut de Chimie Physique, Université Paris-Saclay - CNRS, 91400 Orsay, France;* orcid.org/0000-0001-5752-8461

Chanmin Su − *Bruker Nano Surfaces Division, Santa Barbara, California 93117, United States*

Peter De Wolf − *Bruker Nano Surfaces Division, Santa Barbara, California 93117, United States*

Complete contact information is available at: https://pubs.acs.org/10.1021/acsnano.5c04015

Author Contributions

Concept: C.S., S.H., P.D.W., M.W. Probe design and fabrication: S.H., W.W. Investigation and data analysis: M.W., Q.H., S.H., A.F., P.D.W., A.D. Visualization: M.W. Supervision: C.S., P.D.W., C.P. Writing − original draft: M.W. Writing − review, discussion, and editing: all. All authors have given approval to the final version of the manuscript.

Notes

The authors declare the following competing financial interest(s): All authors except J. M. and A. D. are employed by Bruker Nano Surfaces Division, a manufacturer of instrumentation and probes for AFM-IR spectroscopy. A. D. is a coinventor of AFM-IR patents licensed to Bruker Nano Surfaces Division.

ACKNOWLEDGMENTS

We thank Dr. P. Leclère (Université de Mons) for helpful discussions. We also thank Dr. A. Kurtz, Dr. M. R. Kakuturu, Dr. V. Gorbunov, and Dr. J. Ma for software implementation and support and Dr. S. Redmond for help with the manuscript. A.D. and J.M. acknowledge the support by the Paris Ile-de-France Region-DIM “Matériaux anciens et patrimoniaux”.

REFERENCES

(1) Dazzi, A.; Prater, C. B. AFM-IR: Technology and Applications in Nanoscale Infrared Spectroscopy and Chemical Imaging. *Chem. Rev.* **2017**, *117*, 5146−5173.

(2) Mathurin, J.; Deniset-Besseau, A.; Bazin, D.; Dartois, E.; Wagner, M.; Dazzi, A. Photothermal AFM-IR Spectroscopy and Imaging: Status, Challenges, and Trends. *J. Appl. Phys.* **2022**, *131*, 010901.
(3) Schwartz, J. J.; Jakob, D. S.; Centrone, A. A Guide to Nanoscale IR Spectroscopy: Resonance Enhanced Transduction in Contact and Tapping Mode AFM-IR. *Chem. Soc. Rev.* **2022**, *51*, 5248−5267.
(4) Ramer, G.; Ruggeri, F. S.; Levin, A.; Knowles, T. P. J.; Centrone, A. Determination of Polypeptide Conformation with Nanoscale Resolution in Water. *ACS Nano* **2018**, *12*, 6612−6619.
(5) Ruggeri, F. S.; Mannini, B.; Schmid, R.; Vendruscolo, M.; Knowles, T. P. J. Single Molecule Secondary Structure Determination of Proteins Through Infrared Absorption Nanospectroscopy. *Nat. Commun.* **2020**, *11*, 2945.
(6) Polito, R.; Temperini, M. E.; Ritter, E.; Puskar, L.; Schade, U.; Broser, M.; Hegemann, P.; Baldassarre, L.; Ortolani, M.; Giliberti, V. Conformational Changes of a Membrane Protein Determined by Infrared Difference Spectroscopy Beyond the Diffraction Limit. *Phys. Rev. Appl.* **2021**, *16*, 014048.
(7) Zhu, Q.; Rooney, C. L.; Shema, H.; Zeng, C.; Panetier, J. A.; Gross, E.; Wang, H.; Baker, L. R. The Solvation Environment of Molecularly Dispersed Cobalt Phthalocyanine Determines Methanol Selectivity During Electrocatalytic CO2 Reduction. *Nat. Catal.* **2024**, *7*, 987−999.
(8) Hamadeh, A.; Palmino, F.; Mathurin, J.; Deniset-Besseau, A.; Grosnit, L.; Luzet, V.; Jeannoutot, J.; Dazzi, A.; Chérioux, F. Toward Conformational Identification of Molecules in 2D and 3D Self-Assemblies on Surfaces. *Commun. Chem.* **2023**, *6*, 246.
(9) Ambrosio, A.; Jauregui, L. A.; Dai, S.; Chaudhary, K.; Tamagnone, M.; Fogler, M. M.; Basov, D. N.; Capasso, F.; Kim, P.; Wilson, W. L. Mechanical Detection and Imaging of Hyperbolic Phonon Polaritons in Hexagonal Boron Nitride. *ACS Nano* **2017**, *11*, 8741−8746.
(10) Yoon, Y.; Chae, J.; Katzenmeyer, A. M.; Yoon, H. P.; Schumacher, J.; An, S.; Centrone, A.; Zhitenev, N. Nanoscale Imaging and Spectroscopy of Band Gap and Defects in Polycrystalline Photovoltaic Devices. *Nanoscale* **2017**, *9*, 7771−7780.
(11) Tang, F.; Bao, P.; Su, Z. Analysis of Nanodomain Composition in High-Impact Polypropylene by Atomic Force Microscopy-Infrared. *Anal. Chem.* **2016**, *88*, 4926−4930.
(12) Liu, Y.; Yang, T.; Zhang, B.; Williams, T.; Lin, Y.-T.; Li, L.; Zhou, Y.; Lu, W.; Kim, S. H.; Chen, L.-Q.; Bernholc, J.; Wang, Q. Structural Insight in the Interfacial Effect in Ferroelectric Polymer Nanocomposites. *Adv. Mater.* **2020**, *32*, 2005431.
(13) Jakob, D. S.; Wang, L.; Wang, H.; Xu, X. G. Spectro-Mechanical Characterizations of Kerogen Heterogeneity and Mechanical Properties of Source Rocks at 6 nm Spatial Resolution. *Anal. Chem.* **2019**, *91*, 8883−8890.
(14) Yabuta, H.; Cody, G. D.; Engrand, C.; Kebukawa, Y.; De Gregorio, B.; Bonal, L.; Remusat, L.; Stroud, R.; Quirico, E.; Nittler, L.; Hashiguchi, M.; Komatsu, M.; Okumura, T.; Mathurin, J.; Dartois, E.; Duprat, J.; Takahashi, Y.; Takeichi, Y.; Kilcoyne, D.; Yamashita, S.; et al. Macromolecular Organic Matter in Samples of the Asteroid (162173) Ryugu. *Science* **2023**, *379*, No. eabn9057.
(15) Lu, F.; Jin, M.; Belkin, M. A. Tip-Enhanced Infrared Nanospectroscopy via Molecular Expansion Force Detection. *Nat. Photonics* **2014**, *8*, 307−312.
(16) Kenkel, S.; Mittal, S.; Bhargava, R. Closed-Loop Atomic Force Microscopy-Infrared Spectroscopic Imaging for Nanoscale Molecular Characterization. *Nat. Commun.* **2020**, *11*, 3225.
(17) Katzenmeyer, A. M.; Holland, G.; Kjoller, K.; Centrone, A. Absorption Spectroscopy and Imaging from the Visible through Mid-Infrared with 20 nm Resolution. *Anal. Chem.* **2015**, *87*, 3154−3159.
(18) Tuteja, M.; Kang, M.; Leal, C.; Centrone, A. Nanoscale Partitioning of Paclitaxel in Hybrid Lipid-Polymer Membranes. *Analyst* **2018**, *143*, 3808−3813.
(19) Mathurin, J.; Pancani, E.; Deniset-Besseau, A.; Kjoller, K.; Prater, C. B.; Gref, R.; Dazzi, A. How to Unravel the Chemical Structure and Component Localization of Individual Drug-Loaded Polymeric Nanoparticles by Using Tapping AFM-IR. *Analyst* **2018**, *143*, 5940−5949.
(20) Nowak, D.; Morrison, W.; Wickramasinghe, H. K.; Jahng, J.; Potma, E.; Wan, L.; Ruiz, R.; Albrecht, T. R.; Schmidt, K.; Frommer, J.; Sanders, D. P.; Park, S. Nanoscale Chemical Imaging by Photoinduced Force Microscopy. *Sci. Adv.* **2016**, *2*, No. e1501571.
(21) Dazzi, A.; Palmino, F.; Deniset-Besseau, A.; Mathurin, J.; Luzet, V.; De Wolf, P.; Hu, Q.; Li, C.; Phillips, C.; Chérioux, F. Chemical Mapping of Supramolecular Self-Assembled Monolayers via Atomic Force Microscopy-Based Infrared with a Nanometer-Scale Lateral Resolution. *J. Phys. Chem. Lett.* **2025**, *16*, 3433−3437.
(22) Yang, H. U.; Raschke, M. B. Resonant Optical Gradient Force Interaction for Nano-Imaging and -Spectroscopy. *New J. Phys.* **2016**, *18*, 053042.
(23) O'Callahan, B. T.; Yan, J.; Menges, F.; Muller, E. A.; Raschke, M. B. Photoinduced Tip-Sample Forces for Chemical Nanoimaging and Spectroscopy. *Nano Lett.* **2018**, *18*, 5499−5505.
(24) Jahng, J.; Potma, E. O.; Lee, E. S. Nanoscale Spectroscopic Origins of Photoinduced Tip-Sample Force in the Midinfrared. *Proc. Natl. Acad. Sci. U.S.A.* **2019**, *116*, 26359−26366.
(25) Li, J.; Jahng, J.; Ma, X.; Liang, J.; Zhang, X.; Min, Q.; Wang, X.-L.; Chen, S.; Lee, E. S.; Xia, X.-H. Surface-Phonon-Polariton-Enhanced Photoinduced Dipole Force for Nanoscale Infrared Imaging. *Natl. Sci. Rev.* **2024**, *11*, nwae101.
(26) Menges, F.; Yang, H.; Berweger, S.; Roy, A.; Jiang, T.; Raschke, M. B. Substrate-Enhanced Photothermal Nano-Imaging of Surface Polaritons in Monolayer Graphene. *APL Photonics* **2021**, *6*, 041301.
(27) Jahng, J.; Lee, S.; Hong, S.-G.; Lee, C. J.; Menabde, S. G.; Jang, M. S.; Kim, D.-H.; Son, J.; Lee, E. S. Characterizing and Controlling Infrared Phonon Anomaly of Bilayer Graphene in Optical-Electrical Force Nanoscopy. *Light: Sci. Appl.* **2023**, *12*, 281.
(28) Prine, N.; Cao, Z.; Zhang, S.; Li, T.; Do, C.; Hong, K.; Cardinal, C.; Thornell, T. L.; Morgan, S. E.; Gu, X. Enabling Quantitative Analysis of Complex Polymer Blends by Infrared Nanospectroscopy and Isotopic Deuteration. *Nanoscale* **2023**, *15*, 7365−7373.
(29) Müller, H.; Stadler, H.; De Los Arcos, T.; Keller, A.; Grundmeier, G. AFM-IR Investigation of Thin PECVD SiO_x Films on a Polypropylene Substrate in the Surface-Sensitive Mode. *Beilstein J. Nanotechnol.* **2024**, *15*, 603−611.
(30) Dazzi, A.; Mathurin, J.; Leclere, P.; Nickmilder, P.; De Wolf, P.; Wagner, M.; Hu, Q.; Deniset-Besseau, A. Photothermal AFM-IR Depth Sensitivity: An Original Pathway to Tomographic Reconstruction. *Anal. Chem.* **2024**, *96*, 17931−17940.
(31) Wang, L.; Wang, H.; Xu, X. G. Principle and Applications of Peak Force Infrared Microscopy. *Chem. Soc. Rev.* **2022**, *51*, 5268−5286.
(32) Adamcik, J.; Berquand, A.; Mezzenga, R. Single-Step Direct Measurement of Amyloid Fibrils Stiffness by Peak Force Quantitative Nanomechanical Atomic Force Microscopy. *Appl. Phys. Lett.* **2011**, *98*, 193701.
(33) Young, T. J.; Monclus, M. A.; Burnett, T. L.; Broughton, W. R.; Ogin, S. L.; Smith, P. A. The Use of the PeakForce^{TM} Quantitative Nanomechanical Mapping AFM-Based Method for High-Resolution Young's Modulus Measurement of Polymers. *Meas. Sci. Technol.* **2011**, *22*, 125703.
(34) Pittenger, B.; Erina, N.; Su, C. Mechanical Property Mapping at the Nanoscale Using PeakForce QNM Scanning Probe Technique. In *Nanomechanical Analysis of High Performance Materials*; Tiwari, A., Ed.; Springer Netherlands: Dordrecht, 2014; Vol. *203*, pp 31−51. DOI: 10.1007/978-94-007-6919-9_2
(35) Wang, L.; Wang, H.; Wagner, M.; Yan, Y.; Jakob, D. S.; Xu, X. G. Nanoscale Simultaneous Chemical and Mechanical Imaging via Peak Force Infrared Microscopy. *Sci. Adv.* **2017**, *3*, No. e1700255.
(36) Wang, L.; Wagner, M.; Wang, H.; Pau-Sanchez, S.; Li, J.; Edgar, J. H.; Xu, X. G. Revealing Phonon Polaritons in Hexagonal Boron Nitride by Multipulse Peak Force Infrared Microscopy. *Adv. Opt. Mater.* **2020**, *8*, 1901084.

(37) Ramer, G.; Reisenbauer, F.; Steindl, B.; Tomischko, W.; Lendl, B. Implementation of Resonance Tracking for Assuring Reliability in Resonance Enhanced Photothermal Infrared Spectroscopy and Imaging. *Appl. Spectrosc.* **2017**, *71*, 2013−2020.
(38) Wieland, K.; Ramer, G.; Weiss, V. U.; Allmaier, G.; Lendl, B.; Centrone, A. Nanoscale Chemical Imaging of Individual Chemotherapeutic Cytarabine-Loaded Liposomal Nanocarriers. *Nano Res.* **2019**, *12*, 197−203.
(39) Cappella, B.; Dietler, G. Force-Distance Curves by Atomic Force Microscopy. *Surf. Sci. Rep.* **1999**, *34*, 1−104.
(40) Olubowale, O. H.; Biswas, S.; Azom, G.; Prather, B. L.; Owoso, S. D.; Rinee, K. C.; Marroquin, K.; Gates, K. A.; Chambers, M. B.; Xu, A.; Garno, J. C. "May the Force Be with You!" Force-Volume Mapping with Atomic Force Microscopy. *ACS Omega* **2021**, *6*, 25860−25875.
(41) Hughes, M. L.; Dougan, L. The Physics of Pulling Polyproteins: a Review of Single Molecule Force Spectroscopy Using the AFM to Study Protein Unfolding. *Rep. Prog. Phys.* **2016**, *79*, 076601.
(42) Liu, C.; Pittenger, B.; Hu, S.; Su, C. Force Measurement with Real-Time Baseline Determination. US 9,910,064 B2, 2018.
(43) Giliberti, V.; Badioli, M.; Nucara, A.; Calvani, P.; Ritter, E.; Puskar, L.; Aziz, E. F.; Hegemann, P.; Schade, U.; Ortolani, M.; Baldassarre, L. Heterogeneity of the Transmembrane Protein Conformation in Purple Membranes Identified by Infrared Nanospectroscopy. *Small* **2017**, *13*, 1701181.
(44) Nguyen, H. K.; Shundo, A.; Ito, M.; Pittenger, B.; Yamamoto, S.; Tanaka, K.; Nakajima, K. Insights into Mechanical Dynamics of Nanoscale Interfaces in Epoxy Composites Using Nanorheology Atomic Force Microscopy. *ACS Appl. Mater. Interfaces* **2023**, *15*, 38029−38038.
(45) Killgore, J. P.; DelRio, F. W. Contact Resonance Force Microscopy for Viscoelastic Property Measurements: From Fundamentals to State-of-the-Art Applications. *Macromolecules* **2018**, *51*, 6977−6996.
(46) Rabe, U.; Arnold, W. Acoustic Microscopy by Atomic Force Microscopy. *Appl. Phys. Lett.* **1994**, *64*, 1493−1495.
(47) Rabe, U.; Amelio, S.; Kester, E.; Scherer, V.; Hirsekorn, S.; Arnold, W. Quantitative Determination of Contact Stiffness Using Atomic Force Acoustic Microscopy. *Ultrasonics* **2000**, *38*, 430−437.
(48) Yuya, P. A.; Hurley, D. C.; Turner, J. A. Contact-Resonance Atomic Force Microscopy for Viscoelasticity. *J. Appl. Phys.* **2008**, *104*, 074916.
(49) Killgore, J. P.; Yablon, D. G.; Tsou, A. H.; Gannepalli, A.; Yuya, P. A.; Turner, J. A.; Proksch, R.; Hurley, D. C. Viscoelastic Property Mapping with Contact Resonance Force Microscopy. *Langmuir* **2011**, *27*, 13983−13987.
(50) Pittenger, B.; Yablon, D. G. Quantitative Measurements of Elastic and Viscoelastic Properties with FASTForce Volume CR. *Bruker Application Note* **2017**, 148.
(51) Quaroni, L. Understanding and Controlling Spatial Resolution, Sensitivity, and Surface Selectivity in Resonant-Mode Photothermal-Induced Resonance Spectroscopy. *Anal. Chem.* **2020**, *92*, 3544−3554.
(52) Jakob, D. S.; Schwartz, J. J.; Pavlidis, G.; Grutter, K. E.; Centrone, A. Understanding AFM-IR Signal Dependence on Sample Thickness and Laser Excitation: Experimental and Theoretical Insights. *Anal. Chem.* **2024**, *96*, 16195−16202.
(53) Zhang, Y.; Yilmaz, U.; Lukasievicz, G. V. B.; O'Faolain, L.; Lendl, B.; Ramer, G. An Analytical Model of Label-Free Nanoscale Chemical Imaging Reveals Avenues toward Improved Spatial Resolution and Sensitivity. *Proc. Natl. Acad. Sci. U.S.A.* **2025**, *122*, No. e2403079122.
(54) Efremov, Y. M.; Shpichka, A. I.; Kotova, S. L.; Timashev, P. S. Viscoelastic Mapping of Cells Based on Fast Force Volume and PeakForce Tapping. *Soft Matter* **2019**, *15*, 5455−5463.
(55) Wang, H.; González-Fialkowski, J. M.; Li, W.; Xie, Q.; Yu, Y.; Xu, X. G. Liquid-Phase Peak Force Infrared Microscopy for Chemical Nanoimaging and Spectroscopy. *Anal. Chem.* **2021**, *93*, 3567−3575.
(56) Wang, L.; Wang, H.; Vezenov, D.; Xu, X. G. Direct Measurement of Photoinduced Force for Nanoscale Infrared Spectroscopy and Chemical-Sensitive Imaging. *J. Phys. Chem. C* **2018**, *122*, 23808−23813.

https://doi.org/10.1021/acsnano.5c04015
ACS Nano 2025, 19, 18791−18803